ANNA SZYMCZYK[1),*)], ZBIGNIEW ROSLANIEC[2)]

Non-isothermal crystallization of poly(trimethylene terephthalate)/ single-walled carbon nanotubes nanocomposites

Summary — In this work, non-isothermal crystallization behavior of nanocomposites based on poly(trimethylene terephthalate) (PTT) and single-walled carbon nanotubes (SWCNTs) and neat PTT was studied in order to determine the effects of SWCNTs on its crystallization behavior. Nanocomposites with 0.3 and 0.5 wt. % of SWCNTs were studied. Using of SAXS and DSC methods, the nanostructure of PTT/SWCNTs nanocomposites and neat PTT was investigated in real time in the process of crystallization from the melt. The correlation function approach was used to analyze SAXS data. Changes in long period values, thickness of crystalline lamellae, thickness of amorphous layers, degree of crystallinity during cooling from the melt were discussed.
Keywords: polymer nanocomposites, poly(trimethylene terephthalate), carbon nanotubes.

NIEIZOTERMICZNA KRYSTALIZACJA ZE STOPU NANOKOMPOZYTÓW POLI(TEREFTALAN TRIMETYLENU) / JEDNOŚCIENNE NANORURKI WĘGLOWE

Streszczenie — W pracy omówiono wyniki badań struktury nadcząsteczkowej i własności termicznych nanokompozytów poli(tereftalanu trimetylenu) (PTT) z jednościennymi nanorurkami węglowymi (SWCNTs). Badane nanokompozyty zawierały 0,3 lub 0,5 % mas. SWCNTs. Do oceny dyspersji SWCNTs w matrycy PTT użyto skaningowego mikroskopu elektronowego (SEM). Metodą małokątowego rozpraszania promieni rentgenowskich (SAXS) i metodą różnicowej kalorymetrii skaningowej (DSC) badano nanostrukturę kompozytów PTT/SWCNTs i PTT w czasie rzeczywistym w trakcie krystalizacji ze stopu. Parametry struktury nadcząsteczkowej badanych materiałów wyznaczono na podstawie analizy jednowymiarowych funkcji korelacyjnych. Omówiono zachodzące podczas chłodzenia ze stopu zmiany wartości wielkiego okresu, grubości lamel krystalicznych, grubości obszarów amorficznych oraz stopnia krystaliczności.
Słowa kluczowe: nanokompozyty polimerowe, poli(tereftalan trimetylenu), nanorurki węglowe.

Carbon-based nanomaterials, such as carbon nanotubes (CNTs), are well known for their extraordinarily high mechanical properties (tensile strength up to 150 GPa, Young's modulus higher than 1 TPa) and they have attracted interest as reinforcing fillers for polymer nanocomposites [1—4]. Additionally many superior properties of CNTs such as low weight, very high aspect ratio and high electrical conductivity, make them an attractive candidate to produce advanced composite materials with multifunctional features.

In recent years, CNTs have been used as reinforcements to enhance mechanical and electrical properties of polymeric matrices [1—8]. It is well known that the properties of polymer nanocomposites are strongly depended on the dispersion of nanofillers. The effective use of CNTs in composite applications depends on the ability to disperse the CNTs uniformly throughout the matrix without reducing their aspect ratio. Application of CNTs as a reinforcement has been limited because of their tendency to form ropes or bundles due to strong intertube van der Waals interactions. Bundles can aggregate further, forming entangled networks. Heavily entangled and disordered CNT networks do not have the optimum mechanical, thermal, and electronic properties of individual CNTs.

Previous studies on polyester/CNTs nanocomposites [9—12] has shown that by using *in situ* polymerization method it is possible to obtain composites with low CNTs content and uniform distribution of CNTs in polymer matrix. The obtained nanocomposites based on poly(ethylene terephthalate) (PET) [9—10], poly(butylene terephthalate) (PBT) [11] and poly(trimethylene terephthalate) (PTT) [12] were characterized by improved mechanical properties and low percolation threshold (0.02—0.3 wt. % of CNTs) for electrical conductivity.

[1)] West Pomeranian University of Technology, Faculty of Mechanical Engineering and Mechatronics, Institute of Physics, Al. Piastów 17, 70-310 Szczecin, Poland.

[2)] West Pomeranian University of Technology, Faculty of Mechanical Engineering and Mechatronics, Institute of Materials Science and Engineering, Al. Piastów 17, 70-310 Szczecin, Poland.

[*)] Author for correspondence; e-mail: aszymczyk@zut.edu.pl

In these work, the impact of single-walled carbon nanotubes SWCNTs on the non-isothermal crystallization behavior of PTT nanocomposites was analyzed with DSC and SAXS.

EXPERIMANTAL

Materials

Nanocomposites based on poly(trimethylene terephthalate) (PTT) and single-walled carbon nanotubes (SWCNTs) (CNI Technology Co., TX, USA) with diameter 1.4 nm and several microns in length were prepared with *in situ* polymerization method. Procedure of PTT nanocomposites preparation was the same as previously described for PTT/multi-walled CNTs (PTT/MWCNTs) [12]. Nanocomposites with loading of 0.3 and 0.5 wt. % of SWCNTs were obtained.

Methods of testing

The values of limiting viscosity number ([η]), viscosity-average molecular weight ($\overline{M}_v$) and mass melt flow rate (*MFR*) at temperature 230 °C were determined according to the procedure described in [12, 13].

The morphology of the surface fracture of composite samples was examined with a JEOL JSM-610 scanning electron microscope (SEM). The samples were fractured at liquid nitrogen and gold sputtered prior to observation.

A differential scanning calorimeter (DSC, TA Q 100, TA Instruments) was used to examine the thermal transition of the PTT/SWCNT nanocomposites, in the temperature range from -25 to 250 °C at the heating rate of 10 °C/min under a nitrogen flow of 20 cm^3/min. Samples of approximate mass of 10 mg were encapsulated in aluminum pans. Indium was used as the reference material. Each DSC testing cycle consisted of heating, cooling, and repeating the scans. The first cooling and second heating scans were used to determine the melting and crystallization peaks. The glass transition temperature (T_g) for the polymer samples was taken as the midpoint of the change in heat capacity ($\Delta C_p/2$). The degree of crystallinity x_c (*i.e.* the mass fraction or mass percent of crystallites) was determined as the percent of the integrated heat of fusion (ΔH_m) of the sample in relation to the heat of fusion of fully crystalline PTT, *i.e.* ΔH_m^0 = 146 J/g [14]:

$$x_c = \frac{\Delta H_m}{\Delta H_m^0} \cdot 100\ \% \tag{1}$$

Time-resolved measurements of small X-ray scattering (SAXS) during non isothermal crystallization of PTT nanocomposites were performed at the beam line A2 at HASYLAB (DESY, Hamburg). The wavelength of the X-ray beam was λ = 0.15 nm. Thin samples (~25 mg) sealed between thin aluminum foils were mounted in a Mettler hot stage, which was placed within the X-ray beam path. The sample was first heated to 250 °C. Then it was kept at this temperature for 5 min and cooled to 25 °C at the rate of 3 °C/min. Data from each sample were acquired continuously for 40 s at each temperature, followed by a waiting time of 40 s with a local shutter closed. Linear detectors with delay line readout were used [15]. The SAXS scattering-vectors were calibrated using a dray rat-tail tendon protein. The raw data was corrected for the detector response, then an averaged melt pattern was subtracted from each curve to eliminate background scattering originating from the sample holder and possible other sources, *e.g.*, nanofiller presence, catalyst residues. The intensity SAXS profiles were output as the plot of scattering intensity (*I*) versus scattering vector:

$$s = 2 \sin \theta/\lambda \tag{2}$$

where: 2θ — *scattering angle.*

The position of the scattering maximum (s_{max}), from the Lorentz-corrected SAXS profile, after subtraction of the background, was used for the calculation of the Bragg's long period (L_B), which corresponds to the average distance between the crystalline lamella and amorphous domains:

$$L_B = 1/s_{\max} \tag{3}$$

The SAXS data were analyzed using computer program SAXSDAT [16]. The morphological parameters of the lamellar stacks in the investigated semicrystalline PTT nanocomposites were determined from the linear one-dimensional correlation function $K(r)$ [17—19] which is defined as [17—20]:

$$K(r) = \int_0^\infty I(s)s^2 \cos(2\pi r)\mathrm{d}s \tag{4}$$

where: *I(s) — scattering intensity after background subtraction, r — the distance in real space.*

Before the calculation of the correlation functions, the experimental curves were smoothed using spline functions and then extrapolated to low and high *s* values according to a procedure described in detail elsewhere [19, 20]. Extrapolation to $s = \infty$ was done with the aid of Porod-Ruland model [20, 21]:

$$\lim_{s\to\infty} I(s) = \frac{K}{s^4} e^{-(2\pi\sigma s)^2} + B \tag{5}$$

where: *K — the Porod constant,* σ *— a parameter related to the thickness between the crystalline and amorphous phases, B — background intensity resulting from thermal density fluctuations.*

A typical correlation function for neat PTT is presented in Figure 1. The long period L_c^M was estimated from the position of the first side maximum (see Fig. 1) in the correlation function. According to the procedures described in [18—20] further analysis of the correlation function yields the average crystalline lamellar thickness (l_c) and amorphous layer thickness (l_a). The linear degree of crystallinity (φ_L) was estimated from the correlation function according to the equation:

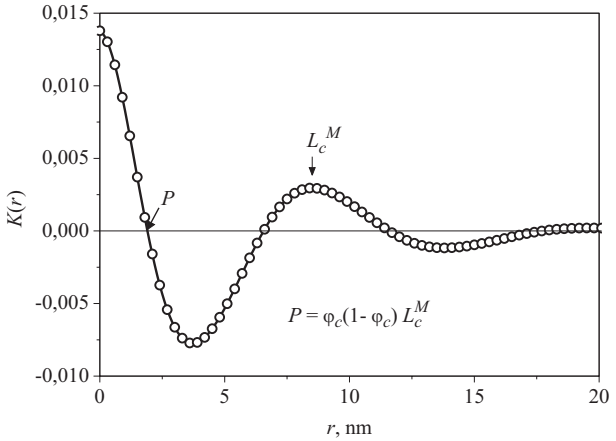

Fig. 1. One-dimensional correlation function typical of all the PTT samples, and the long period (L_c^M) determined from the correlation functions

$$\frac{P}{L_c^M} = \varphi_L(1-\varphi_L) \tag{6}$$

where: P — *the ordinate corresponding to the first zero of the abscissa in the correlation function (see Fig. 1).*

The volume fraction of crystallinity (φ_c) of the sample can be calculated from relationship [22]:

$$\varphi_c = \alpha_s \cdot \varphi_L \tag{7}$$

where: α_s — *the total volume of the sample occupied by stacks of lamellae.*

The crystalline and amorphous layer thickness can be calculated from:

$$l_c = \varphi_L L_c^M \tag{8}$$

$$l_a = (1-\varphi_L) L_c^M \tag{9}$$

RESULTS AND DISCUSSION

Characterization of the PTT/SWCNTs nanocomposites

Dispersion of carbon nanotubes in PTT matrix was evaluated by SEM analysis of cryofractured surfaces of nanocomposites. The representative morphologies of the PTT/MWCNT nanocomposites with the highest concentration of SWCNTs are shown in Figure 2. The SEM image shows that the SWCNTs were rather uniformly dispersed in the PTT matrix, despite some small entanglements in SWCNTs structures.

Characteristics of the obtained nanocomposites are presented in Table 1.

The obtained PTT nanocomposites have average molecular weight close to the neat PTT. The values of the mass melt flow rate (*MFR*) of nanocomposites are lower than that of neat PTT, indicating their higher melt viscosity. Higher melt viscosity of nanocomposites in comparison to the neat PTT suggest the existence of interconnected or network structures formed as a result of CNT-polymer and CNT-CNT interactions. The increase

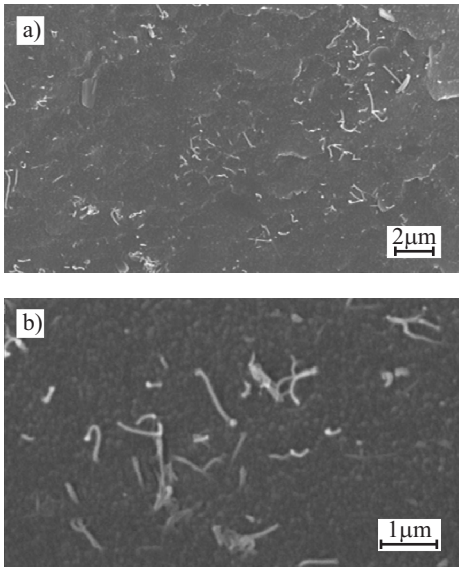

Fig. 2. SEM of PTT/SWCNTs nanocomposites with 0.5 wt. % of SWCNTs for original magnification: a) 5000, b) 15 000

of melt viscosity in the presence of CNTs is the reason that the *in situ* polymerization method can be used to obtain nanocomposites with low CNTs loading. The highest content of SWCNTs achieved in the prepared PTT nanocomposites was 0.5 wt. %. The introduction of higher content of SWCNTs was not possible because the melt does not flow.

T a b l e 1. Characteristics of neat PTT and prepared PTT/SWCNTs nanocomposites; meaning of the symbols is explained in the text

Symbol of the sample	Content of SWCNTs, wt. %	[η] dL/g	$\overline{M}_v$ g/mol	*MFR* g/min
PTT	—	0.82	41 400	17.1
PTT/0.3	0.3	0.80	40 000	16.4
PTT/0.5	0.5	0.81	40 600	14.5

Effect of SWCNTs on PTT crystallization

The effect of SWCNTs on the crystallization of PTT was analyzed with a non-isothermal DSC experiment which results are presented in Figure 3. Figure 3a shows the DSC cooling scans of neat PTT and nanocomposites containing SWCNTs.

The crystallization onset temperature ($T_{c,on}$) and crystallization peak temperature (T_c) determined during cooling from the melt at 10 °C/min, the glass transition temperature (T_g) and peak melting temperature (T_m) recorded during a subsequent heating DSC scan at 10 °C/min and the degree of crystallinity (x_c) obtained after cooling the sample from the melt are presented in Table 2. During cooling from the melt, the nanocomposites showed crystallization exotherms with higher $T_{c,on}$ and T_c, these can indicate the efficiency of SWCNTs as strong

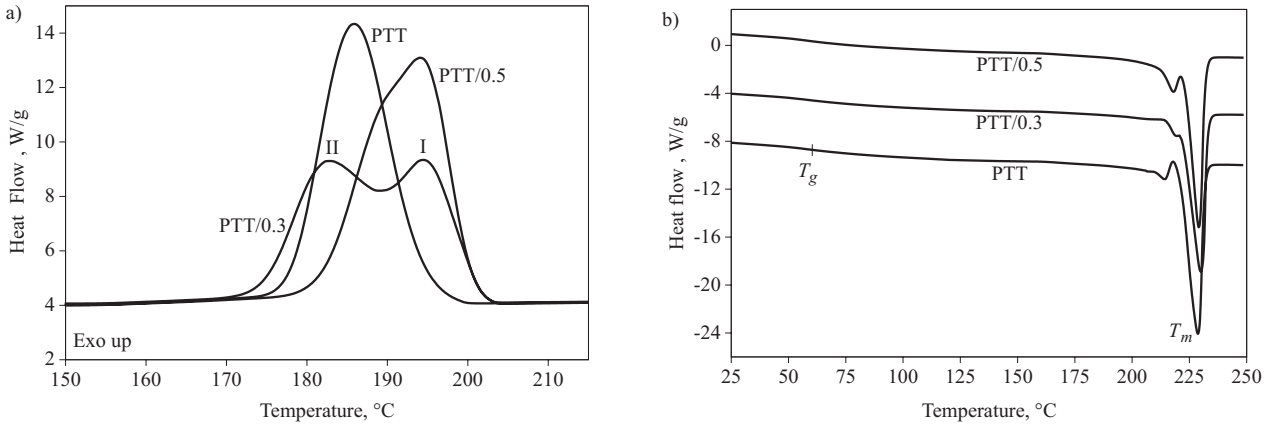

Fig. 3. DSC thermograms obtained during cooling (a) and heating (b) for PTT and PTT/SWCNTs nanocomposites

T a b l e 2. Thermal parameters for neat PTT and PTT/SWCNTs nanocomposites determined using DSC; meaning of the symbols is described in the text

Symbol of the sample	T_g, °C	ΔC_p, J/g °C	T_m, °C	ΔH_m, J/g	T_c, °C	$T_{c,on}$, °C	ΔH_c, J/g	x_c, %
PTT	51	0.19	229	53.1	194	185	53.4	36.4
PTT/0.3	52	0.18	230	55.2	202	195, 182	55.7	37.8
PTT/0.5	52	0.19	229	56.2	202	194	56.9	38.5

nucleation agents for crystallization of PTT. For PTT nanocomposite with 0.3 wt. % of SWCNTs double exothermic peak (I, II) was observed. As the loading of SWCNTs increase, the $T_{c,on}$ does not increase indicating that it is possible saturation of the nucleation efficiency at low SWCNTs concentration. This can be related to the large surface area and good dispersion of SWCNTs. The addition of CNTs had no effect on T_g and ΔC_p of amorphous phase of semicrystalline PTT. The reduction of and ΔC_p is usually due to lower mobility of the polymer chains, which might be expected in the highly loaded and exfoliated CNT. The melting point is not affected by addition of CNTs. The degree of crystallinity of PTT nanocomposites negligibly increases (1.4—2 %) in comparison to the neat PTT. The obtained here results are contrary to the results obtained by Ma and Cebe [23] for PTT composite nanofibers containing multi-walled carbon nanotubes. For these nanocomposites the slight decrease of crystallinity and T_g with the amount of MWCNTs was found. Based on the three-phase model, including presence of a mobile fraction (MAF), rigid fraction (RAF) and crystalline fraction in semicrystalline PTT [23, 24], it was established that addition of MWCNTs enhanced the PTT chain alignment and increased RAF as a result. The presence of MWCNTs has induced interfacial interactions between nanotubes and the polymer matrix which may have caused a strong restriction on the polymer chains. As a result, the reduction in segmental mobility would tend to increase RAF. The existence of the third phase, RAF, in PTT/MWCNTs nanocomposites was strongly supported by their FT-IR analysis [23]. In PTT two kinds of conformational isomers exist *i.e. gauche* (G) and *trans* (T). According to the results presented in literature [23] in crystalline regions only *gauche* conformers exist, while in amorphous region mainly *trans* conformers occur. While the degree of crystallinity and mobile amorphous fraction decreased (according to DSC results) as CNTs loading increased, the increase in *gauche* conformers in the nanocomposites with increase of MWCNTs loading was found. The addition of MWCNTs inhibits the formation of *trans* conformers. These results suggest that in RAF rigid amorphous fraction the *gauche* and *trans* conformers exist, but in MAF mainly *trans* conformers exist. Previous results [12] have shown that introduction of COOH functionalized MWCNTs in PTT matrix caused decrease in the rate of PTT crystallization, indicating that the functionalization of CNTs weakens the heterogeneous nucleation effect of the nanotubes. A similar effect has been reported in the literature for PA6 [25] and poly(ethylene oxide) (PEO) MWCNTs nanocomposites [26, 27]. All these results concerning crystallization behavior of PTT/CNTs composites have shown that the type of carbon nanotubes and their surface modification can affect the crystallization behavior of PTT.

Crystallization of PTT/SWCNTs nanocomposites analyzed by SAXS

Effect of the presence of SWCNTs in PTT matrix on the evolution of the lamellar nanostructure was monitored by SAXS during non-isothermal crystallization. Figure 4 shows representative time-resolved Lorentz corrected SAXS profiles of neat PTT and PTT/SWCNTs nanocomposites obtained during non-isothermal crystallization at 3 °C/min. It can be seen that SAXS curves exhibit a distinct diffraction maxima confirming that PTT crys-

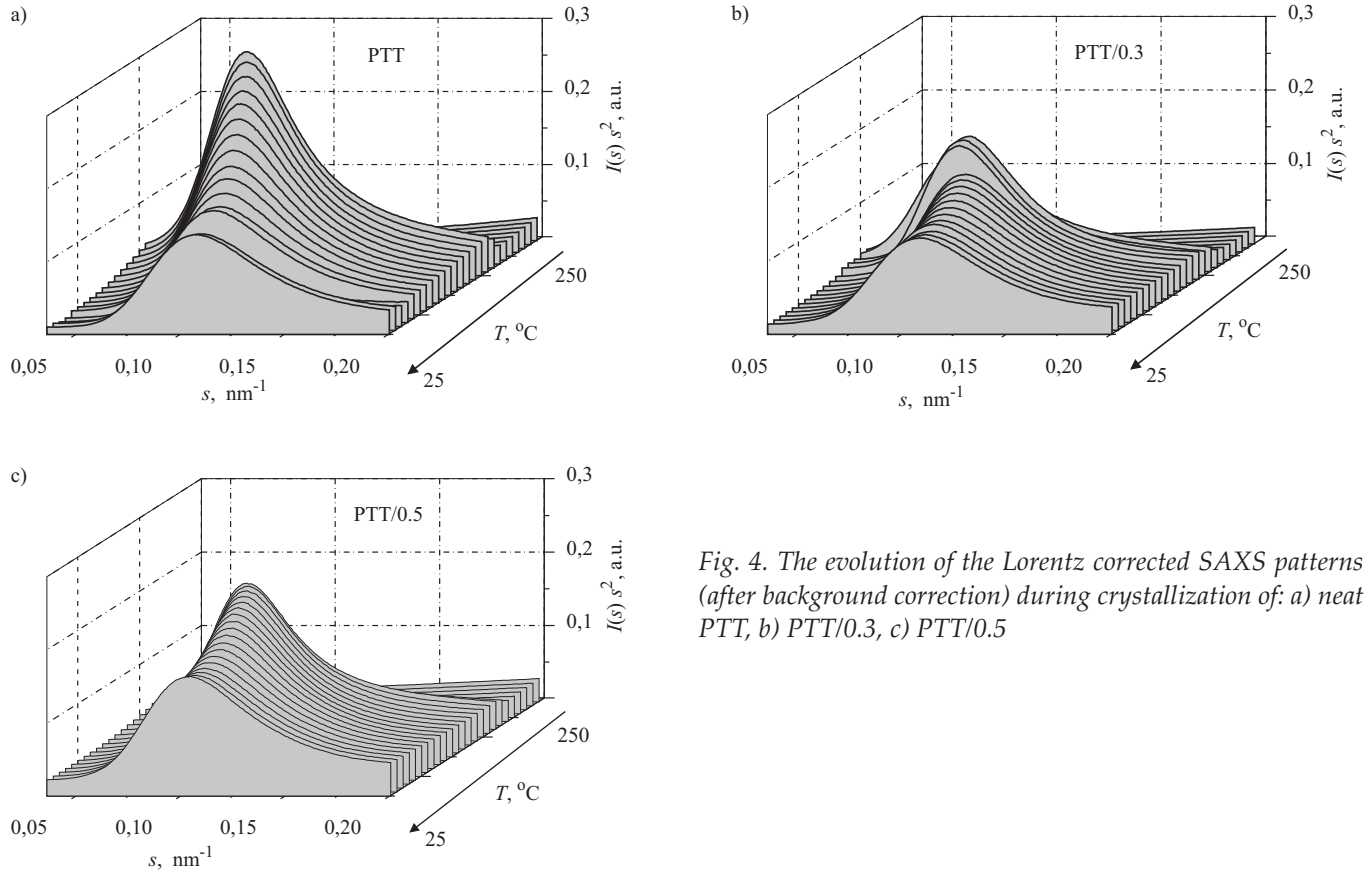

Fig. 4. The evolution of the Lorentz corrected SAXS patterns (after background correction) during crystallization of: a) neat PTT, b) PTT/0.3, c) PTT/0.5

tallizes into a distribution of lamellar crystals separated by amorphous regions.

The first maximum position at the initial temperature (178 °C) on SAXS curves for nanocomposites are located at 0.075 nm^{-1} (PTT/0.3) and 0.081 nm^{-1} (PTT/0.5) corresponding to the Bragg's long period (L_B) values of 13.3 nm and 12.3 nm, respectively. For neat PTT the first maximum (at 160 °C) appears at 0.084 nm^{-1} corresponding to the long period value of L_B = 11.8 nm. During the crystallization of PTT and PTT/SWCNTs nanocomposites the position of the intensity maximum shifts to higher scattering vector s, corresponding to the lower values of L_B.

The correlation function [$K(r)$] has been applied to follow the changes of the nanostructure of PTT/SWCNTs composites and neat PTT during crystallization. Figure 5 displays the evolution of $K(r)$ functions for neat PTT and nanocomposite (PTT/0.5) during cooling. According to procedure reported in [19, 20] analysis of the $K(r)$ allows to determine: L_c^M, l_c, l_a and crystallinity within the lamellar stacks (ϕ_L).

Figure 6 summarizes the results of the nanostructure studies during melt crystallization of neat PTT and nanocomposites. The difference between L_c^M (Fig. 6a) and l_c gives l_a. At higher temperatures a significant decrease of

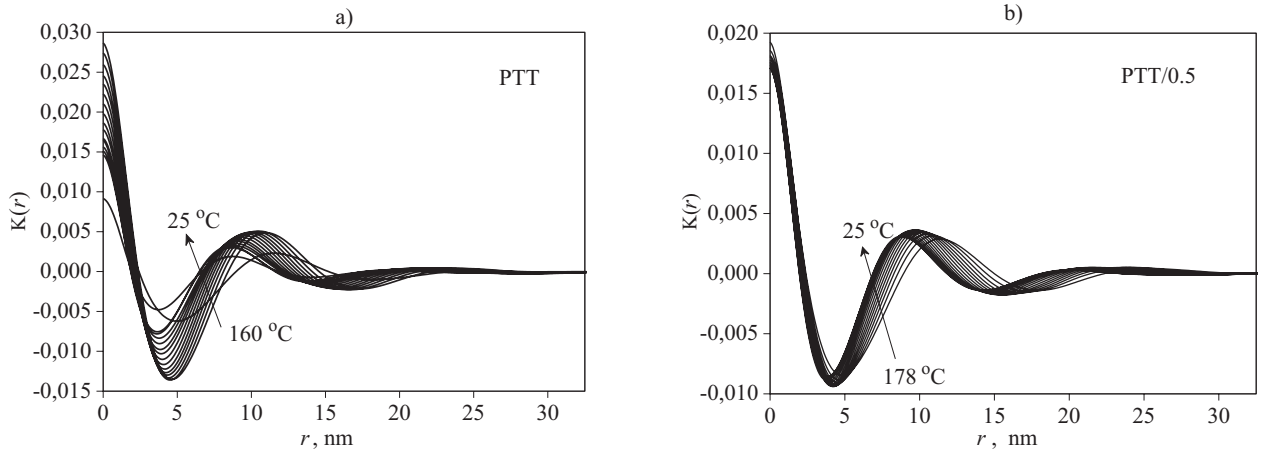

Fig. 5. Evolution of one-dimensional correlation functions at different temperatures during cooling for: a) neat PTT, b) PTT/0.5 nanocomposite

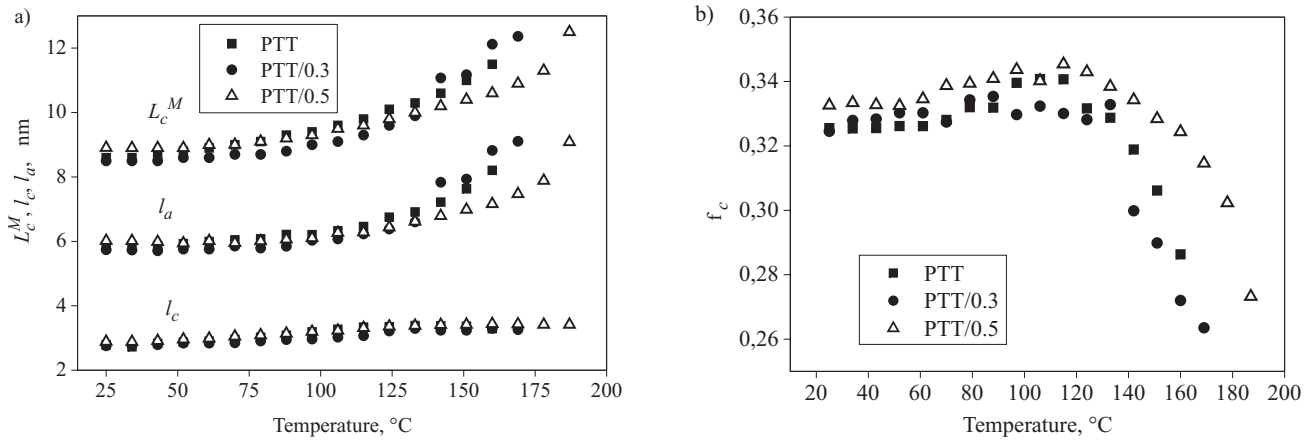

Fig. 6. The nanostructure parameters determined from correlation functions for neat PTT and PTT/SWCNTs nanocomposites during cooling: a) long period (L_c^M), thickness of rystalline lamellae (l_c) and amorphous layer (l_a), b) fraction of crystallinity (ϕ_c)

L_c^M accompanied by the decrease of the l_a for neat PTT and nanocomposites is observed. At the same time the significant increase of the linear crystallinity (ϕ_L) (Fig. 6b) of all the samples is observed. This is consistent with the appearance of lamellar stacks filling in the sample volume. The observed initial decrease can be connected with the sequential formation of either new crystal lamellae or lamellar stacks or both in the interlamellar amorphous regions [28]. Finally, nanocomposites show the comparable values of the long period (L_c^M = 8.5 nm for PTT/0.3 and L_c^M = 8.9 nm for PTT/0.5) and the linear crystallinity (ϕ_L = 0.323 for PTT/0.3 and ϕ_L = 0.333 for PTT/0.5) in comparison to the neat PTT (L_c^M = 8.6 nm, ϕ_L = 0.325, see Fig. 6). Nanocomposites have comparable thickness of crystalline lamellae as neat PTT. Slightly higher value of L_c^M for composite with 0.5 wt. % loading of SWCNTs stems from the thickener amorphous layer.

According to a assumption that stacks of lamellae are volume-filing in the semicrystalline polymer the linear crystallinity determined by SAXS should be identical to the bulk crystallinity measured with the DSC and WAXS methods.

The differences in the value of crystallinity of neat PTT and nanocomposites determined by DSC (x_c, mass fraction) and SAXS ($\phi_c = \alpha_s \phi_L$ [22], volume fraction) can result from different thickness of the samples and cooling rate applied during the analysis. Independent information concerning crystallinity of the neat PTT sample (prepared at the same conditions) was used to decide which solution of eq. (6) was reflected to the „real" value of local volume crystallinity.

The amorphous and crystal PTT has density of 1.299 g/cm^3 and 1.432 g/cm^3 [14], respectively. Using the method of Goderis *at al.* [22] and Swan's [29] relations for densities of amorphous and crystalline phases, the volume fraction crystallinity were transformed into a mass fraction crystallinity and compared with the value obtained from the wide-angle X-ray diffraction (WAXS) method. Here, the obtained for neat PTT value of mass fraction crystallinity x_c(SAXS) = 0.346 is very close to the calculated x_c(WAXS) = 0.342 determined by WAXS method as described in our previous study [13], and slightly lower than the determined by DSC (x_c = 0.364). The obtained results for neat PTT confirm that the applied here model of crystalline-amorphous two-phase lamellar system can correctly describe the real structure of investigated PTT and PTT/SWCNTs nanocomposites.

CONCLUSIONS

PTT nanocomposites containing 0.3 or 0.5 wt. % of SWCNTs were obtained by *in situ* polycondensation. The obtained nanocomposites show uniform dispersion of SWCNTs in polymer matrix. In comparison to the neat PTT, the glass transition temperature and meting temperature of PTT in nanocomposites are not significantly influenced by the presence of SWCNTs. The SWCNTs displayed a clear nucleating effect on the PTT crystallization due to the increase in the crystallization onset temperature and crystallization peak temperature of nanocomposites compared to neat PTT. The degree of crystallinity of the nanocomposites is comparable to the neat PTT. From SAXS data it was found that the long period of PTT/SWCNTs nanocomposites is similar to the neat PTT.

ACKNOWLEDGMENT

The authors thank for the financial support from the Polish National Science Centre within the grant No. 2183/B/T02/2011/40.

The experiments performed at A2 at HASYLAB (DESY) were done using the beamtime of the proposal II-20080143EC. We thank Mr Sérgio S. Funari for support during measurements at HASYLAB and Mrs Elżbieta Piesowicz for her assistance in the time-resolved experiments.

REFERENCES

1. O'Connell M. J.: „Carbon Nanotubes Properties and Applications", CRC Press Taylor & Francis Group Boca Raton 2006, pp. 214—250.

2. Moniruzzaman M., Winey K. I.: *Macromolecules* 2006, **39**, 5194.
3. Paul D. R., Robeson L. M.: *Polymer* 2008, **49**, 3187.
4. Hernández J. J., García-Gutiérrez M. C., Nogales A., Rueda D. R., Sanz A., Sics I., Hsiao B. S., Roslaniec Z., Broza G., Ezquerra T. A.: *Polymer* 2007, **48**, 3286.
5. Bikiaris D.: *Materials* 2010, **3**, 2884.
6. Qian D., Dickey E. C., Andrews R., Rantell T.: *Appl. Phys. Lett.* 2000, **76**, 2868.
7. Bai J. B., Allaoui A.: *Composites Part A: Appl. Sci. Manufact.* 2003, **34**, 689.
8. Müller A. J., María Luisa Arnal M. L., Trujillo M., T. Lorenzo A. T.: *Eur. Polym. J.* 2011, **47**, 614.
9. Hernández J. J., García-Gutiérrez M. C., Nogales A., Rueda D. R., Kwiatkowska M., Szymczyk A., Roslaniec Z., Concheso A., Guinea I., Ezquerra T. A.: *Comp. Sci. Technol.* 2009, **69**, 867.
10. Gómez-del Río T., Poza P., Rodríguez J., García-Gutiérrez M. C., Hernández J.J., Ezquerra T. A.: *Comp. Sci. Technol.* 2010, **70**, 284.
11. Nogales A., Broza G., Roslaniec Z., Schulte K., Sics I., Hsiao B. S., Santz A., García-Gutiérrez M. C, Rueda D. R., Domingo C., Ezquerra T. A.: *Macromolecules* 2004, **37**, 7669.
12. Szymczyk A., Roslaniec Z., Zenker M., García-Gutiérrez M. C., Hernández J. J., Rueda D. R., Nogales A., Ezquerra T. A.: *eXPRESS Polymer Letters* 2011, **5**, 977.
13. Szymczyk A.: *Eur. Polym. J.* 2009, **45**, 2653.
14. Scheirs J., Long, T. E.: „Modern polyester: chemistry and technology of polyesters and copolyesters", John Wiley Sons, Chichester 2004, pp. 361—397.
15. Boulin C. J., Kempf R., Gabriel A., Koch M. H. J.: *Nucl. Instrum. Meth. Phys. Res.* 1988, **A269**, 312.
16. Rabiej S., Rabiej M.: „A computer program SAXDAT for the analysis of the SAXS scattering curves of semicrystalline polymers", ATH, Bielsko-Biała 2009, pp. 13—46.
17. Strobl G. R., Schneider M.: *J. Polym. Sci.: Polym. Phys. Ed.* 1980, **18**, 1343.
18. Strobl G. R., Schneider M. J., Voight-Martin I. G.: *J. Polym. Sci. Part A* 1980, **18**, 1361.
19. Hsiao B. S., Verma R. K.: *J. Synchr. Rad.* 1998, **5**, 23.
20. Rabiej S.: „Zastosowanie metody SAXS w badaniach struktury nadcząsteczkowej polimerów semikrystalicznych", ATH, Bielsko-Biała 2009, pp. 17—60.
21. Ruland W. J.: *J. Appl. Crystallogr.* 1971, **4**, 70.
22. Goderis B., Reynaers H., Koch M. H., Mathot V. B. F.: *J. Polym. Sci. Part B* 1999, **37**, 1715.
23. Ma Q., Cebe P.: *J. Therm. Anal. Calorim.* 2010, **102**, 425.
24. Pyda M., Wunderlich B.: *J. Polym. Sci.: Part B: Polym. Phys.* 2000, **38**, 622.
25. Li J., Fang Z., Tong L., Gu A., Liu F.: *J. Polym. Sci. Part B: Polym. Phys.* 2006, **44**, 1499.
26. Goh H. W, Goh S. W., Xu G. Q., Pramoda K. P., Zhang W. D.: *Chem. Phys. Lett.* 2003, **379**, 236.
27. Jin J., Song M., Pan F.: *Thermochim. Acta* 2007, **456**, 25.
28. Sanz A., Nogales A., Ezquerra T. A., Soccio M., Munari A., Lotti N.: *Macromolecules* 2010, **43**, 671.
29. Swan P. R.: *J. Polym. Sci.* 1960, **42**, 525.

Received 19 VII 2011.